Nanoscale

PAPER

Cite this: *Nanoscale*, 2019, **11**, 8380

Proton-irradiation-immune electronics implemented with two-dimensional charge-density-wave devices†

A. K. Geremew, [a] F. Kargar, [a] E. X. Zhang, [b] S. E. Zhao, [b] E. Aytan,[a] M. A. Bloodgood,[c] T. T. Salguero,[c] S. Rumyantsev, [a,d] A. Fedoseyev,[e] D. M. Fleetwood [b] and A. A. Balandin *[a]

Received 22nd February 2019,
Accepted 8th April 2019

DOI: 10.1039/c9nr01614g

rsc.li/nanoscale

We demonstrate that charge-density-wave devices with quasi-two-dimensional 1T-TaS_2 channels show remarkable immunity to bombardment with 1.8 MeV protons to a fluence of at least 10^{14} H^+cm^{-2}. The current–voltage characteristics of these devices do not change as a result of proton irradiation, in striking contrast to most conventional semiconductor devices or other two-dimensional devices. Only negligible changes are found in the low-frequency noise spectra. The radiation immunity of these "all-metallic" charge-density-wave devices is attributed to the quasi-2D nature of the electron transport in the nanoscale-thickness channel, high concentration of charge carriers in the utilized charge-density-wave phases, and two-dimensional device design. Such devices, capable of operating over a wide temperature range, can constitute a crucial segment of future electronics for space, particle accelerator and other radiation environments.

The future of space exploration depends crucially on the development of new electronic technologies that are immune to space radiation, which consists primarily of protons, electrons, and cosmic rays.[1–4] The penetrating energetic radiation of deep space produces negative impacts on not only biological entities but also the electronic systems of space vehicles. Proton radiation damage is an important failure mechanism for electronic devices in near-Earth orbits, deep space and high energy physics facilities.[1–4] Protons can cause ionizing damage and atomic displacements, resulting in device degradation and malfunction.[5–10] Shielding of electronics increases the weight and cost of the systems but does not eliminate destructive single events produced by energetic protons.[8,10] Electronics capable of operating in high-radiation environments are also needed for monitoring nuclear materials, medical diagnostics, radiation treatments, nuclear reactors and particle accelerators.[5–12] Modern electronics based on semiconductors – even those specially designed for radiation hardness – remain highly susceptible to proton damage.

High-energy proton irradiation causes ionizing damage by generating excess charges at the interface regions in the complementary metal–oxide-semiconductor (CMOS) transistors and other typical microelectronic devices and integrated circuits.[8–14] This type of damage results in the changes in the threshold voltages and source–drain currents, potentially leading to device or system failure. Protons also can induce displacement damage, which typically leads to the formation of point and cluster defects in semiconductors. Some of these defects introduce electronic trapping states that often reveal themselves by increases in low-frequency noise (LFN).[15,16] Noise increases beyond system tolerance limits is therefore an additional challenge to electronics in high-radiation environments. Heavy shielding, or the use of conventional radiation-hardened technologies and backup devices, increases system complexity and costs, while not providing complete protection from proton-induced damage. This situation motivates the exploration of new materials and innovative device designs that are immune to proton irradiation.

A promising approach for developing radiation-immune electronics is the use of CDW effects, which appear in some metallic systems.[17] For many years, classical CDW materials like the bulk quasi-one-dimensional (1D) metals $NbSe_3$ and $TaSe_3$ were considered interesting from the physics point of

[a]*Nano-Device Laboratory, Department of Electrical and Computer Engineering, Materials Science and Engineering Program, University of California, Riverside, California 92521, USA. E-mail: balandin@ece.ucr.edu; https://balandingroup.ucr.edu/*
[b]*Department of Electrical Engineering and Computer Science, Vanderbilt University, Nashville, Tennessee 37235, USA*
[c]*Department of Chemistry, University of Georgia, Athens, Georgia 30602, USA*
[d]*Center for Terahertz Research and Applications, Institute of High-Pressure Physics, Polish Academy of Sciences, Warsaw, 01-142 Poland*
[e]*Ultra Quantum Inc., Huntsville, Alabama 35758, USA*

†Electronic supplementary information (ESI) available. See DOI: 10.1039/c9nr01614g

view but impractical owing to the low temperatures of the CDW phase transitions. Recently, however, their status has changed. New studies have demonstrated that transitions between the incommensurate (IC) and nearly commensurate (NC) CDW states in some quasi-2D materials, which happen above RT, can be triggered effectively by electric field.[18] Specifically, 1T-TaS_2 shows a transition from the NC-CDW to IC-CDW phase at 350 K. An electric field applied along the device channel can trigger the NC-to-IC phase transition, accompanied by an abrupt change in the electrical conductivity and hysteresis loop, at various temperatures.[19–21] Additional work has shown that such CDW current–voltage, *I–V*, characteristics can be utilized for implementing voltage controlled oscillators (VCO), modulators and logic gates.[18,22,23] These studies also suggest that CDW devices can be low-power[22,23] and extremely fast-up to terahertz frequencies.[18]

Metals are inherently more radiation tolerant than semiconductors owing to much higher carrier densities, *i.e.* $n_e \geq 10^{20}$ cm^{-3} in metals *vs.* 10^{10} cm^{-3}–10^{19} cm^{-3} in semiconductors. One can also expect that the quasi-2D geometry of the channels and two-terminal structure of CDW devices will make them less susceptible to radiation damage within a given environment, owing to their reduced interaction volumes. Thus, the most important test for the radiation hardness of quasi-2D CDW devices is investigation of their susceptibility to proton irradiation. In this study, we show that CDW devices with quasi-2D 1T-TaS_2 channels, operating at RT, reveal high immunity to 1.8 MeV proton radiation of up to a fluence of at least 10^{14} P^+ cm^{-2}. This discovery demonstrates the promise of CDW devices for use in critical electronic systems for space exploration and other radiation environments.

For this study, high-quality 1T-TaS_2 crystals were prepared by the chemical vapor transport method (see ESI†). To avoid air oxidation and chemical contamination, devices with 1T-TaS_2 channels and Ti/Au contacts were fabricated using the shadow mask method (see Methods). To investigate the intrinsic radiation hardness, we intentionally did not use a hexagonal boron nitride (h-BN) channel capping, which is a typical design approach for quasi-2D devices. The schematic, layered structure, typical *I–V* characterization with load resistance, and oscillations resulting from a properly biased 1T-TaS_2 device are shown in Fig. 1a. An optical microscopy image of an array of 1T-TaS_2 devices with different CDW channel lengths is presented in Fig. 1b.

RT proton irradiation was performed under vacuum conditions using the Vanderbilt Pelletron.[24] To allow for better comparison with the prior reports on other devices, we selected a proton energy of 1.8 MeV. Experiments were performed at fluences of 1×10^{12} cm^{-2}, 3×10^{12} cm^{-2}, 1×10^{13} cm^{-2}, 3×10^{13} cm^{-2}, and 1×10^{14} cm^{-2}. The flux for the proton irradiation was around 5×10^{10} protons (s^{-1} cm^{-2}). Because the non-ionizing energy loss of 1.8 MeV protons is

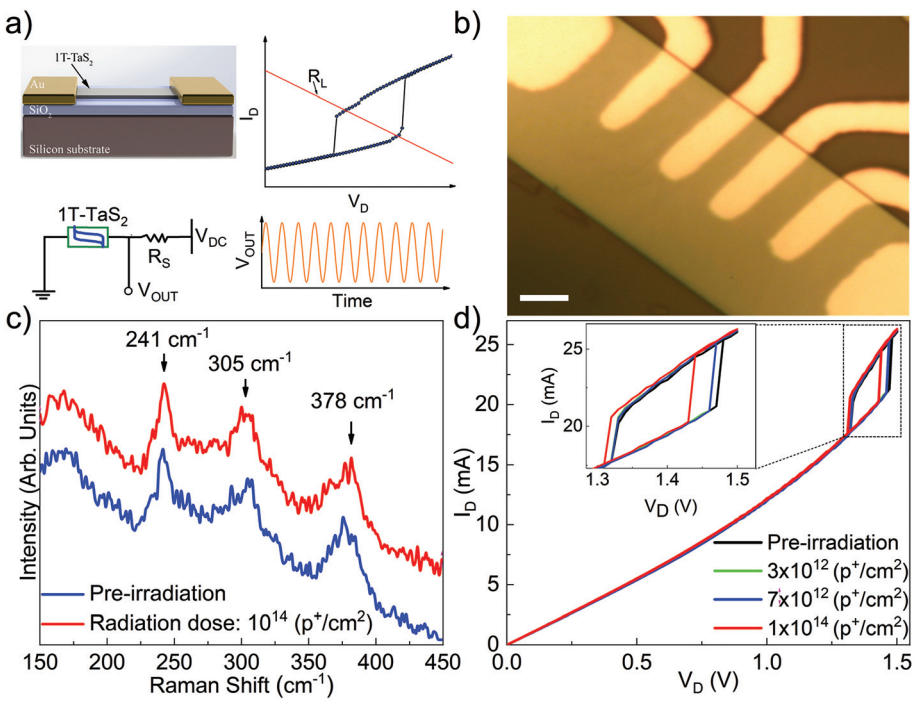

Fig. 1 Charge-density-wave device structure and characteristics. (a) Schematic diagram of the two-terminal 1T-TaS_2 CDW device, its typical current–voltage characteristic, oscillator output and symbol representation (clockwise). (b) An optical microscopy image of fabricated 1T-TaS_2 device with Ti/Au (10 nm/100 nm) contacts. The scale bar is 3 μm. (c) Raman spectra of 1T-TaS_2 channel before (blue line) and after (red line) proton irradiation. No changes, which would indicate possible material damage, are observed. (d) Current–voltage characteristics of 1T-TaS_2 device after different proton fluences. The inset shows the hysteresis window, which is the working part of the *I–V* characteristic of the device. The changes in the current and voltage are negligible even after the maximum proton irradiation dose.

much higher than that of the higher-energy protons,[25,26] the equivalent total-ionizing and displacement damage doses in this study are quite high compared with any realistic space environments.[27] Indeed, the highest investigated proton fluences in the present study (up to 10^{14} P^+ cm^{-2}) are comparable to the highest doses potentially experienced in nuclear reactor loss-of-coolant accidents or future high-luminosity particle accelerator applications. Details of the proton testing are provided in the Methods. The *I–V* characteristics were checked after each irradiation step for several devices. After the final proton fluence, LFN characteristics were measured. Raman spectroscopy and transmission electron microscopy were used to assess possible damage to 1T-TaS_2 channels. Fig. 1c shows Raman spectra of 1T-TaS_2 before and after proton irradiation to a total fluence of 10^{14} cm^{-2}. The spectra did not show any signs of the crystal lattice damage. In Fig. 1d, we present *I–V* characteristics of the representative quasi-2D 1T-TaS_2 CDW device before irradiation and after different proton radiation doses.

The measured *I–V* characteristics clearly show the linear low-field region followed by the hysteresis due to the NC-CDW to IC-CDW transition, consistent with all prior reports on such devices.[18–23] The hysteresis region is the functional part of *I–V* curves, essential for operation of the CDW VCOs and logic gates[18,22,23] (see Fig. 1a). For comparison with other materials and technologies, it is convenient to analyze the relative changes in the current, $\Delta I/I$, and voltage, $\Delta V/V$, due to irradiation. In conventional devices, I is the source–drain current, while V is the threshold, V_T, or drain, V_D, voltage. In our case, V is the onset of the resistive switching, which is a close analog of V_T, and I is the corresponding current (see the limiting values in the hysteresis loop). Naturally, $\Delta I/I \approx 1$ indicates an extremely high radiation damage while $\Delta I/I \approx 0$ means no damage. Analyzing Fig. 1d one can sees that quasi-2D CDW devices do not show any noticeable proton radiation damage, even after a total fluence of 10^{14} cm^{-2} of 1.8 MeV protons. The functional hysteresis window preserves its shape after all irradiation steps; changes in the relevant *I–V* characteristics were as low as $\Delta I/I < 10^{-5}$ and $\Delta V/V < 1.4 \times 10^{-5}$. These values are extremely small compared to all other 2D devices reported in the literature. Table 1 provides a comparison of 1T-TaS_2 CDW devices to the best devices implemented with other 2D materials and tested for proton irradiation damage.[28–32] The total ionizing dose (TID) and the charge carrier concentration, n, are either taken directly from the reports or calculated from the data provided. One should note that all other 2D devices use a field-effect transistor (FET) concept, which make them more susceptible to proton and X-ray damage due to charge trapping in surrounding insulators or at the device-insulator interfaces. Additional reference information for radiation damage, including X-rays and gamma-rays, for all types of devices are provided in the ESI.†

Table 1 Proton bombardment effects on quasi-2D devices

2D devices	n (cm^{-2})	$\Delta I/I$	$\Delta V/V$	TID rad (SiO_2)	Energy (MeV)	Ref.
1T-TaS_2	10^{18}	3×10^{-5}	1.4×10^{-5}	2.0×10^{8}	1.80	This work
Graphene	10^{13}	1.00	0.99	4.0×10^{9}	5.00	28
Graphene	10^{13}	0.33	—	4.0×10^{8}	15.0	29
Graphene	10^{13}	0.67	0.99	2.0×10^{10}	5.00	30
MoS_2	10^{12}–10^{13}	1.00	1.00	2.0×10^{8}	10.0	31
WSe_2	10^{12}–10^{13}	0.11	0.99	2.0×10^{8}	2.00	32

The negligible changes in $\Delta I/I$ and $\Delta V/V$ confirm insignificant total ionizing damage. To examine other possible negative effects of proton bombardment, *e.g.* displacement damage, we conducted LFN measurements, following standard protocols (see Methods). The high-energy, high-fluence proton irradiation of the device channel can result in physical displacement of atoms leading to creation of defects. The higher density of defects, with various time constants, often results in increased LFN, irrespective of its mechanism, *i.e.* carrier number *vs.* mobility fluctuations.[15,16] This relationship emphasizes the importance of LFN spectroscopy for assessing the radiation damage related to defect creation.[10] Fig. 2a shows the voltage-referred noise power spectral density, S_V, as a function of frequency, f, for several voltage biases, V_D, before proton irradiation and after the final irradiation step (10^{14} P^+ cm^{-2} bombardment). All noise spectra are of the $1/f$ type without any traces of generation – recombination bulges. The most important observation is that the noise level hardly changes after high-dose proton irradiation. The current noise spectral density, S_I, is presented as a function of current, I, in Fig. 2b. It is known from the noise theory that S_I proportionality to I^2 is indicative of conventional $1/f$ noise, without signs of Joule heating, electromigration or material degradation. Fig. 2c and d show the *I–V* characteristics and the normalized noise spectral density, S_I/I^2 (f = 10 Hz) of the quasi-2D 1T-TaS_2 device after proton bombardment, as a function of the applied voltage, V_D. The inset to Fig. 2c shows the low-bias resistivity as a function of temperature across the NC to IC CDW phase transition. The overall LFN level is rather low, $S_I/I^2 \sim 10^{-12}$ Hz^{-1}–10^{-10} Hz^{-1}, compared to mature conventional technologies,[15] and reaches a maximum at V_D = 1.4 V. A comparison of Fig. 2c and d indicates that the noise peak is associated with the IC to NC CDW phase transition, which is demonstrated here to be unaffected by proton bombardment. LFN attains its maxima at phase transitions, which explains its significance as a spectroscopy tool for CDW effects.[33]

To understand better the proton bombardment immunity of quasi-2D 1T-TaS_2 CDW devices, we performed simulation of the impact of proton irradiation using the stopping and range of ions in solids (SRIM) software tools.[34] The SRIM method is based on the Monte Carlo approach with the binary collision approximation and random selection of the impact parameters of the colliding ions.[34,35] The simulated device structure consisted of the layers of 1T-TaS_2 (90 nm), SiO_2 (300 nm) and Si (10 μm), subjected to a 1.8 MeV proton beam. The simulation results suggest that the damage caused by atomic displacements is quite low, at the level of 10^{-6} per ion. This means that the long-term device characteristics are not impaired even under high proton irradiation. Protons primarily pass through

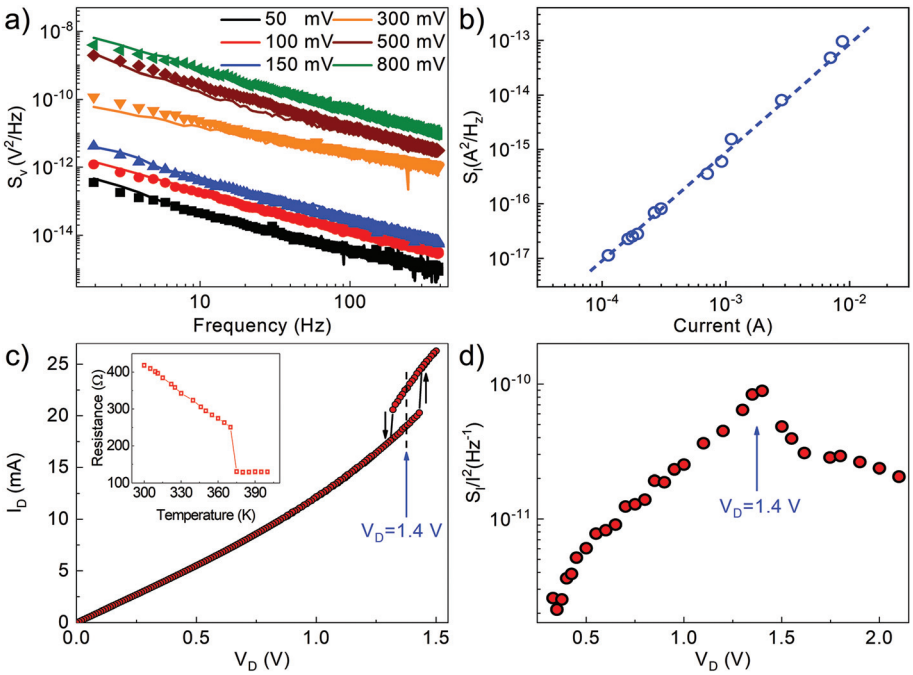

Fig. 2 Low-frequency noise and *I*–*V* characteristics of the charge-density-wave devices. (a) The noise voltage power spectral density, S_V, as a function of frequency for a representative 1T-TaS_2 device before (solid lines) and after (symbols) proton irradiation. (b) Noise current power spectral density, S_I, as a function of the source–drain current, *I*, indicating the noise scales as I^2. Data are shown for the device after the maximum proton irradiation dose, at the frequency f = 10 Hz. (c) Current–voltage characteristics of 1T-TaS_2 device after proton irradiation to 10^{14} P^+ cm^{-2}, showing that the hysteresis window is preserved. The inset illustrates the temperature change of the resistance. (d) The normalized current noise spectral density, S_I/I^2, as a function of the source–drain bias. Note that the noise reaches its maximum level at a voltage of 1.4 V, which corresponds to the hysteresis window of the near-commensurate to incommensurate phase transition presented in the panel (c).

the 1T-TaS_2 device channel without causing damage and deposit their energy in the Si substrate. The average energy lost to recoils, on the order of 1 meV, is insignificant compared to the initial proton energy of 1.8 MeV. The simulation data are presented in the ESI.†

Considering the data in Table 1 and the results of SRIM simulations, one can attribute the proton radiation immunity of CDW devices to the thin-film structure of the active channel, the two-terminal design, and the high concentration of the charge carriers in metallic 1T-TaS_2. The protons penetrate the thin film channel without causing significant damage and deposit most of their energy in the depth of Si substrate, without affecting the device operation. The same process happens in quasi-2D FETs.[29–32,36,37] However, since graphene and MoS_2 FETs rely on gate bias for their operation, even small charge accumulation in the surrounding dielectric layers or at the interface can lead to substantial changes in $\Delta I/I$ and $\Delta V/V$. Similar considerations apply to carbon nanotube FETs, with the best radiation hardened devices attaining $\Delta I/I \approx 0.06$ and $\Delta V/V \approx 0.08$ under 40 keV X-ray irradiation to 2×10^6 rad(SiO_2),[38] a change more than two orders of magnitude larger than that experienced by devices in this work. The quasi-2D CDW 1T-TaS_2 devices are two-terminal, operated by changing the in-plane voltage bias. The load resistor is connected in series, and is made of inherently radiation-tolerant metal. The absence of the traditional gate and gate dielectric removes components susceptible to radiation damage mechanisms related to dielectric or surface charge accumulation. The high concentration of carriers in 1T-TaS_2, both in NC and IC CDW states, which is comparable to metals, further reduces possible fluctuations in $\Delta I/I$ and $\Delta V/V$ owing to defect creation and electron trapping. In comparison to other two-terminal resistive switching devices, the CDW devices perform better due to their quasi-2D thin-film channel design and substantially higher carrier densities. The radiation hardness of conventional, well-established devices technologies, such as Si CMOS, GaN and SiC FETs varies considerably depending on the device design, dimensions and special radiation hardness provisions. Typical $\Delta V/V$ values for the conventional technologies are in the range 0.005–0.99,[6–14] which are substantially larger than those observed for the quasi-2D 1T-TaS_2 CDW devices. Even for devices showing high radiation tolerance, complex and expensive testing protocols are required for device qualification, which is not the case for these CDW devices.[10,16,39,40] This immunity to proton bombardment of quasi-2D CDW devices confirms and greatly extends past studies that demonstrated hardness to X-rays at ionizing doses more than two orders of magnitude lower than those experienced in this study.[41]

In conclusion, we demonstrated that quasi-2D CDW devices have remarkable immunity to irradiation by high-energy protons. The *I*–*V* and LFN analysis show no significant

changes up to at least the high fluence of 10^{14} $H^{+}cm^{-2}$, indicating the absence of both total-ionizing-dose and displacement-damage effects. The radiation immunity of the CDW devices is attributed to their two-terminal design, quasi-2D nature of the active channel, and the high concentration of the charge carriers. The results show that these devices are quite promising for the design of future radiation-hard electronics for critical systems required in the extremely high radiation environments associated with space applications, particle accelerators, nuclear reactors, and other extreme environments.

Methods

1T-TaS_2 crystal growth

Millimeter-sized crystals of 1T-TaS_2 were grown *via* chemical vapor transport (CVT). Elemental Ta (Sigma-Aldrich), elemental S (J.T. Baker), and elemental I_2 (J.T. Baker) were added to a fused quartz ampoule. The ampoule was evacuated and backfilled three times with argon, with cooling to mitigate I_2 sublimation. The ampoule was flame-sealed and heated in a two-zone tube furnace at 10 °C min^{-1} to 975 °C (hot zone) and 875 °C (cool zone). Then the ampoule was removed from the hot furnace and immediately quenched in a water–ice–NaCl bath. The structure and phase purity of the 1T-TaS_2 were verified with powder X-ray diffraction and HRTEM, and the correct stoichiometry was confirmed by energy dispersive spectroscopy.

Device fabrication

The devices were fabricated by the shadow mask method to avoid damage from chemical contamination typically associated with conventional lithographic lift-off processes. The shadow masks were fabricated using double-side polished Si wafers with 3 μm thermally grown SiO_2 on both sides (Ultrasil Corp.; p-type; <100>). The details of the mask fabrication process have been reported elsewhere.[42,43] At the next step, the shadow masks were used to fabricate several devices by aligning the masks with the pre-selected layers of 1T-TaS_2 under an optical microscope. The aligned mask and device substrate were clamped together and placed in an electron beam evaporator (EBE) for contact deposition (10 nm Ti and 100 nm Au) through the mask openings. The completed devices were then transferred to another vacuum chamber for electrical characterization. The thickness and width of 1T-TaS_2 layers were determined using the atomic force microscopy (AFM) and scanning electron microscopy (SEM).

Electronic noise measurements

The noise spectra were measured using a dynamic signal analyzer (Stanford Research) and a semiconductor analyzer (Keysight). The measurements were conducted in the two-terminal device configuration. Since the contact resistance of the devices was low, the noise response was dominated by the contribution from the active device channel contribution. The extracted contact noise from the transmission line measurement structures was substantially below the thermal noise, which had no significant contribution to the channel noise. The dynamic signal analyzer measured the absolute voltage noise spectral density, S_V, of a parallel resistance network of a load resistor, R_L, and device under test, R_D. The normalized current noise spectral density, S_I, was calculated from the equation: $S^2 = S_V \times [(R_L + R_D)/(R_L \times R_D)]^2/(G^2)$, where G is the amplification of the low-noise amplifier.

Proton irradiation

1.8 MeV proton irradiation testing was conducted under vacuum at RT using the Vanderbilt Pelletron.[24] For reference, the range of 1.8 MeV protons is ~20 μm in Si, ensuring that the protons are sufficiently energetic to penetrate all device layers.[44] All devices were irradiated with both terminals grounded during test to avoid potential current-induced annealing of displacement damage.[45] The DC I–V measurements were conducted using a HP4156B semiconductor parameter analyzer during both the irradiation and noise measurement sequences. Forward and reverse sweeps were performed to observe the hysteresis window. One terminal was grounded during the I–V measurements, and the bias range for the other terminal was decided by the NC to IC CDW transition point. Details of the proton irradiation testing have been reported elsewhere in the context of other material systems.[10,16]

Contributions

A.A.B. conceived the idea, coordinated the project, contributed to experimental data analysis and led the manuscript preparation; A.G. fabricated devices and contributed to the experimental data analysis; E.X.Z. and S.E.Z. conducted proton irradiation testing and noise measurements; M.A.B. conducted material synthesis and characterization; T.T.S. supervised material synthesis and contributed to materials characterization; D.M.F. supervised proton irradiation testing and noise measurements, and contributed to data analysis; S.R. contributed to noise and radiation data analysis; E.A. conducted Raman and TEM material characterization. A.F. performed simulation of proton irradiation. All authors contributed to manuscript preparation.

Conflicts of interest

There are no conflicts to declare.

Acknowledgements

The work at UCR and UGA was supported, in part, by the National Science Foundation (NSF) Emerging Frontiers of Research Initiative (EFRI) 2-DARE project: Novel Switching Phenomena in Atomic MX_2 Heterostructures for Multifunctional Applications (NSF EFRI-1433395). A. A. B. also acknowledges the UC – National Laboratory Collaborative

Research and Training Program – University of California Research Initiatives (LFR-17-477237). Nanofabrication was performed in the Center for Nanoscale Science and Engineering (CNSE) Nanofabrication Facility at UC Riverside. The work at Vanderbilt University was supported, in part, by U.S. Air Force Office of Scientific Research (AFOSR) through the Hi-REV program. S. R. also acknowledges partial support from the Center for Terahertz Research and Applications co-financed with the European Regional Development Fund. A. G. and A. A. B. thank Dr Guanxiong Liu for useful discussions on fabrication of the CDW devices. D. M. F. also thanks M. W. McCurdy for experimental assistance.

References

1 R. J. White and M. Averner, Humans in space, *Nature*, 2001, **409**, 1115.
2 E. Gibney, How to build a Moon base, *Nature*, 2018, **562**, 474–478.
3 E. Adli, *et al.*, Acceleration of electrons in the plasma wakefield of a proton bunch, *Nature*, 2018, **561**, 363–367.
4 T. Ghidini, Materials for space exploration and settlement, *Nat. Mater.*, 2018, **17**, 846–850.
5 M. A. Xapsos, *et al.*, Probability model for worst case solar proton event fluences, *IEEE Trans. Nucl. Sci.*, 1999, **46**, 1481–1485.
6 A. H. Johnston, *et al.*, Proton degradation of light-emitting diodes, *IEEE Trans. Nucl. Sci.*, 1999, **46**, 1781–1789.
7 F. Faccio, *et al.*, TID and displacement damage effects in vertical and lateral power MOSFETs for integrated DC-DC converters, *IEEE Trans. Nucl. Sci.*, 2010, **57**, 1790–1797.
8 R. D. Schrimpf, *et al.*, Radiation effects in new materials for nano-devices, *Microelectron. Eng.*, 2011, **88**, 1259–1264.
9 Z. Zhang, *et al.*, Thermal stability of deep level defects induced by high energy proton irradiation in n-type GaN, *J. Appl. Phys.*, 2015, **118**, 155701.
10 D. M. Fleetwood, Evolution of total ionizing dose effects in MOS devices with Moore's law scaling, *IEEE Trans. Nucl. Sci.*, 2018, **65**, 1465–1481.
11 G. S. Was, *et al.*, Emulation of reactor irradiation damage using ion beams, *Scr. Mater.*, 2014, **88**, 33–36.
12 A. Šagátová, *et al.*, Radiation hardness of GaAs sensors against gamma-rays, neutrons and electrons, *Appl. Surf. Sci.*, 2017, **395**, 66–71.
13 R. Jiang, *et al.*, Worst-case bias for proton and 10 keV X-ray irradiation of AlGaN/GaN HEMTs, *IEEE Trans. Nucl. Sci.*, 2017, **64**, 218–225.
14 N. E. Ives, *et al.*, Effects of proton-induced displacement damage on GaN HEMTs in RF power amplifier applications, *IEEE Trans. Nucl. Sci.*, 2015, **62**, 2417–2422.
15 A. A. Balandin, *Noise and Fluctuations Control in Electronic Devices, 03*, World Scientific Publishing Co., 2003.
16 D. M. Fleetwood, 1/*f* noise and defects in microelectronic materials and devices, *IEEE Trans. Nucl. Sci.*, 2015, **62**, 1462–1486.
17 G. Grüner, The dynamics of charge-density waves, *Rev. Mod. Phys.*, 1988, **60**, 1129–1181.
18 G. Liu, *et al.*, A charge-density-wave oscillator based on an integrated tantalum disulfide–boron nitride–graphene device operating at room temperature, *Nat. Nanotechnol.*, 2016, **11**, 845.
19 Y. Yu, *et al.*, Gate-tunable phase transitions in thin flakes of 1T-TaS_2, *Nat Nanotechnol.*, 2015, **10**, 270–276.
20 A. W. Tsen, *et al.*, Structure and control of charge density waves in two-dimensional 1T-TaS_2, *Proc. Natl. Acad. Sci. U. S. A.*, 2015, **112**, 15054–15059.
21 L. Ma, *et al.*, A metallic mosaic phase and the origin of Mott-insulating state in 1T-TaS_2, *Nat. Commun.*, 2016, **7**, 10956.
22 A. Khitun, G. Liu and A. A. Balandin, Two-dimensional oscillatory neural network based on room temperature charge-density-wave devices, *IEEE Trans. Nanotechnol.*, 2017, **16**, 1–8.
23 A. G. Khitun, A. K. Geremew and A. A. Balandin, Transistorless logic circuits implemented with 2-D charge density wave devices, *IEEE Electron Device Lett.*, 2018, **39**, 1449–1452.
24 M. W. McCurdy, *et al.*, *Vanderbilt Pelletron – Low energy protons and other ions for radiation effects on electronics*, *in 2015 IEEE Radiation Effects Data Workshop (REDW)*, 2015, pp. 146–151.
25 G. P. Summers, E. A. Burke, P. Shapiro and S. R. Messenger, Damage correlations in semiconductors exposed to gamma, electron, and proton irradiations, *IEEE Trans. Nucl. Sci.*, 1993, **40**, 1372–1379.
26 J. Chen, *et al.*, Effects of applied bias and high field stress on the radiation response of GaN/AlGaN HEMTs, *IEEE Trans. Nucl. Sci.*, 2015, **62**, 2423–2430.
27 M. A. Xapsos, P. M. O'Neill and T. P. O'Brien, Near-Earth space radiation models, *IEEE Trans. Nucl. Sci.*, 2014, **60**, 1691–1705.
28 G. Ko, *et al.*, Electrical characterization of 5 MeV proton-irradiated few layer graphene, *Electrochem. Solid-State Lett.*, 2010, **13**, 32–34.
29 S. Lee, *et al.*, Proton irradiation energy dependence of defect formation in graphene, *Appl. Surf. Sci.*, 2015, **344**, 52–56.
30 C. Lee, *et al.*, Strong hole-doping and robust resistance-decrease in proton-irradiated graphene, *Sci. Rep.*, 2016, **6**, 21311.
31 T.-Y. Kim, *et al.*, Irradiation effects of high-energy proton beams on MoS_2 field effect transistors, *ACS Nano*, 2014, **8**, 2774–2781.
32 P. Dhakras, *et al.*, TID effects in reconfigurable MOSFETs using 2-D semiconductor WSe_2, *IEEE Trans. Nucl. Sci.*, 2018, **65**, 53–57.
33 G. Liu, S. Rumyantsev, M. A. Bloodgood, T. T. Salguero and A. A. Balandin, Low-frequency current fluctuations and sliding of the charge density waves in two-dimensional materials, *Nano Lett.*, 2018, **18**, 3630–3636.
34 J. F. Ziegler and J. P. Biersack, *The Stopping and Range of Ions in Matter BT – Treatise on Heavy-Ion Science: Volume 6:*

Astrophysics, Chemistry, and Condensed Matter, Springer, US, 1985.
35 A. Fedoseyev, *et al.*, Accurate numerical models for simulation of radiation events in nano-scale semiconductor devices, *Math. Comput. Simul.*, 2008, **79**, 1086–1095.
36 E. X. Zhang, *et al.*, Low-energy X-ray and ozone-exposure induced defect formation in graphene materials and devices, *IEEE Trans. Nucl. Sci.*, 2011, **58**, 2961–2967.
37 R. C. Walker, *et al.*, Radiation effects on two-dimensional materials, *Phys. Status Solidi A*, 2016, **213**, 3065–3077.
38 C. D. Cress, *et al.*, Radiation effects in single-walled carbon nanotube papers, *J. Appl. Phys.*, 2010, **107**, 14316.
39 F. Faccio, *et al.*, Influence of LDD spacers and H+ transport on the total-ionizing-dose response of 65 nm MOSFETs irradiated to ultrahigh doses, *IEEE Trans. Nucl. Sci.*, 2018, **65**, 164–174.
40 G. Borghello, *et al.*, Dose-rate sensitivity of 65 nm MOSFETs exposed to ultrahigh doses, *IEEE Trans. Nucl. Sci.*, 2018, **65**, 1482–1487.
41 G. Liu, *et al.*, Total-ionizing-dose effects on threshold switching in 1T-TaS_2 charge density wave devices, *IEEE Electron Device Lett.*, 2017, **38**, 1724–1727.
42 A. K. Geremew, S. Rumyantsev, M. A. Bloodgood, T. T. Salguero and A. A. Balandin, Unique features of the generation–recombination noise in quasi-one-dimensional van der Waals nanoribbons, *Nanoscale*, 2018, **10**, 19749–19756.
43 A. Geremew, *et al.*, Current carrying capacity of quasi-1D $ZrTe_3$ van der Waals nanoribbons, *IEEE Electron Device Lett.*, 2018, **39**, 735–738.
44 NIST Physical Measurement Laboratory, Stopping-power & range tables for electrons, protons, and helium ions, https://www.nist.gov/pml/stopping-power-range-tables-electrons-protons-and-helium-ions, last accessed April 5, 2019.
45 J. R. Srour, C. J. Marshall and P. W. Marshall, Review of displacement damage effects in silicon devices, *IEEE Trans. Nucl. Sci.*, 2003, **50**, 653–670.